Simulations of nanopore formation and phosphatidylserine externalization in lipid membranes subjected to a high-intensity, ultrashort electric pulse

Q. Hu, R. P. Joshi, and K. H. Schoenbach
Department of Electrical and Computer Engineering, Old Dominion University, Norfolk, Virginia 23529-0246, USA
(Received 24 March 2005; published 8 September 2005)

A combined MD simulator and time dependent Laplace solver are used to analyze the electrically driven phosphatidylserine externalization process in cells. Time dependent details of nanopore formation at cell membranes in response to a high-intensity (100 kV/cm), ultrashort (10 ns) electric pulse are also probed. Our results show that nanosized pores could typically be formed within about 5 ns. These predictions are in very good agreement with recent experimental data. It is also demonstrated that defect formation and PS externalization in membranes should begin on the anode side. Finally, the simulations confirm that PS externalization is a nanopore facilitated event, rather than the result of molecular translocation across the trans-membrane energy barrier.

DOI: 10.1103/PhysRevE.72.031902 PACS number(s): 87.15.Aa, 87.50.Rr, 87.50.−a, 87.17.Aa

I. INTRODUCTION

The use of very high electric fields (~100 kV/cm or higher) with pulse durations in the nanosecond range [1–3] has been a very recent development in bioelectrics. Traditionally, most electroporation studies have focused on relatively low external electric fields (less than a kilovolt per centimeter), applied over time periods ranging from several tens of microseconds to milliseconds [4]. From a practical standpoint, nanosecond pulsed electric fields (nsPEFs) could be useful for various biological applications ranging from cellular electroporation [5–7], the production of hybridomas [8,9], injection of xenomolecules such as hormones, proteins, RNA, DNA and chromosomes [10–16], the electrofusion of dielectrophoretically aligned cells [17,18], and the nonthermal destruction of microorganisms [19–21]. In *ex vivo* studies, electroporation has been used to load drugs. Manipulation of the oxygen binding capability [22] and the electroinsertion of proteins [23] have also been carried out. *In vivo* applications have included the delivery of potent anticancer drugs into solid tumors [24,25].

There appear to be inherent advantages in using short electric pulses. These include: (i) Negligible thermal heating, (ii) the ability to develop large electric fields and peak powers, with a lower energy input, and most importantly, (iii) the capacity to create large transmembrane potentials across subcellular organelles, such as the mitochondria. As has been recently reported, voltage variations across the mitochondrial membrane can induce cytochrome *c* release via a two-step process [26,27]. The likely channel involves a field-induced disruption in the electrostatic binding of cytochrome *c* with the inner mitochondrial membrane. The details have not been studied, and the dynamics remain unclear. However, this release does trigger the activation of various caspases, and apoptotic cell death ultimately results. Thus, deliberate and targeted apoptotic cell killing (e.g., of tumor cells) can potentially be achieved through the use of an ultrashort, high-intensity electrical pulse.

The following salient features have emerged from various recent studies of cellular responses to high-intensity (~100 kV/cm), nanosecond electric pulses. (i) Apoptosis has been observed [28,29] for cells with the behavior depending on pulse duration. Thus, for example, cells subjected to various external electric fields at a constant energy level, showed strongest apoptosis markers for the longer (~300 ns) pulses, less at the shorter (~60 ns) durations, and almost negligible effects for a short 10 ns pulse [29]. A recent model based on an energy-landscape approach [30] yielded results qualitatively in keeping with these observations. (ii) Multiple pulses have been observed to do more irreversible damage than single-shot electric shocks. (iii) Externalization of phosphatidylserine (PS) was shown to occur in response to a nanosecond pulse for average electric fields above 2 MV/m [31,32]. A distinct polarity effect has been observed, with the externalization predominantly occurring at the anode end. PS is an acidic phospholipid that is normally located on the inner leaflet of the lipid bilayer. The PS translocation event essentially marks cells for macrophage scavenging and ultimate death. However, the mechanism remains to be studied, and the dynamical process details will be addressed here. (iv) Calcium is released from the intracellular endoplasmic reticulum in response to external voltage pulses [6,33–35]. This could be a vital element in induction or possible suppression of cell signaling.

Much of the biophysical analysis related to such field-dependent phenomena has generally been based on static, continuum models. For example, predictions of pore growth and evolution utilize a voltage controlled, pore formation energy function that is spatially independent [3,36,37], and does not account for structural changes. Similarly, static energy barrier concepts (e.g., the Born energy [38] are invoked for ion transport across membranes, and for PS flip-flop transitions occurring in lipid bilayers [39]. Such a static picture is inaccurate because of the inherent fluctuations and voltage-driven dynamical changes in the molecular structure. Furthermore, since such external field driven processes occur under highly nonequilibrium conditions, the application of simple thermodynamics and Markovian response breaks down.

An essential task here is to accurately model the collective physics at the molecular level due to the externally ap-

plied, high-field, short-duration macrovoltages. For realistic simulations it is important to address two aspects simultaneously. First, the time dependent electric fields, created at the cell membrane by the external voltage waveform applied to remote electrodes, need to be obtained. This field provides the dynamic driving force for the membrane molecules, internal dipoles and surrounding water. Second, the dynamical evolution of the membrane nanostructure under the influence of this dynamic field and the many-body interactions need to be adequately treated. Here, the first aspect has been addressed through a Laplace solver coupled with the Smoluchowski equation for the time dependent potential distribution. This yields a dynamic electric field and transmembrane voltage at a membrane patch. A molecular dynamics approach has then been applied to the membrane patch (taken to correspond with the polar region of a cell) to evaluate the molecular response. In most other simulations of this type for chemical and biological applications [40–42], there is no externally applied voltage. Only a few recent reports [43,44] have considered the effect of electric fields on biomembranes. However, in those cases, a constant electric field had been assumed. In the present context, actual nanosecond ($\sim$10 ns) pulses are routinely applied in our laboratory [29,35], and so any realistic modeling necessitates the inclusion of time-varying transmembrane voltages.

An important goal of this contribution is the analysis of PS externalization that has been observed with nsPEF application. In healthy cells, PS is almost exclusively located on the inner plasma membrane of eukaryotic cells [45]. This skewed spatial distribution is maintained by a Ca^{2+} inhibited, adenosine triphosphate (ATP) -dependent aminophospholipid translocase [46], and a Ca^{2+} dependent aminophospholipid scramblase [47,48]. The translocation of PS on the outer leaflet is an important physiological signal that marks the cell for phagocytosis, and even plays a role in platelet activation and blood coagulation [49]. The physical mechanism remains unclear, though a calcium-aided process [34], a possible nonporative dipole interaction mechanism [50], and porative diffusion [51] have all been suggested. Here it is demonstrated that the PS externalization process for the ultrashort, high-intensity situation is simply the result of nanopore formation in the plasma membrane, followed by the drift and diffusion of the charged PS molecules. The anodic-side externalization can be understood as arising from the anode-side preference for nanopore formation. The directionality of electrical forces on the negatively charged PS molecules also contributes. Though there could well be other chemically driven processes [34,50], including interactions between PS and reactive oxygen species [52], here we focus purely on the electrical pathway.

II. MODELING DETAILS

In order to facilitate meaningful comparisons with actual experiments, two important aspects have to be considered. First, the microscopic electric field across an actual membrane has to be determined from an experimentally averaged value representing the global voltage applied across the entire sample. Typically, such electric-pulse experiments are carried out by placing a buffered mixture containing the cells in a microcuvette. Thus only the spatially averaged electric field is known from the applied voltage input and physical separation between electrodes. The task of determining the microscopic membrane voltage at a microscopic patch from the global value was carried out here by an analytical model, as discussed in the next section. A second important point is that the microscopic membrane field is time dependent and hence, the temporal details need to be included within the MD simulations. Here, this was obtained dynamically by coupling a Laplace solver with the Smoluchowski equation. This yielded a dynamic transmembrane voltage, which was discretized in time as a step function, and used as an input to the MD code.

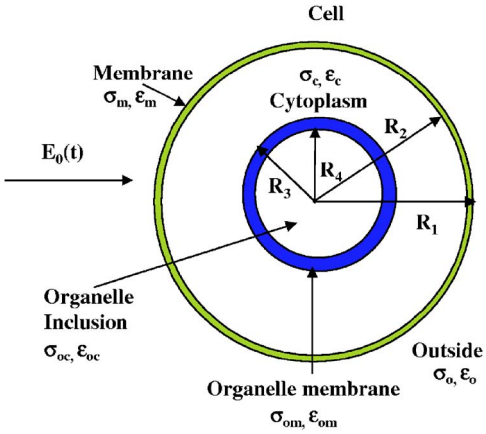

FIG. 1. (Color online) Schematic of the cell model for the transmembrane potential calculations.

A. Time dependent transmembrane potential calculations

One possible approach to calculating the transmembrane potential is through a time-domain nodal analysis involving a distributed equivalent circuit representation of a cell and its membrane structures. Details of this method have been discussed in our previous papers [30,53,54]. Here we present a more computationally efficient way based on a coupled solution of the Laplace equation and current continuity equations at each time step. The external electric field $E(t)$ was taken to be along the z axis, and to have the exact time-dependent shape corresponding to the external waveform. The schematic shown in Fig. 1 represents a cell suspended in a medium. The geometric model is similar to that used by Grosse and Schwan [55] for analyzing potentials induced by alternating fields. The cell in Fig. 1 is characterized by radius R_1 and thickness R_1-R_2. The outer region has an assigned conductivity σ_o and permittivity ϵ_o, while the corresponding parameters for the cell membrane are σ_m and ϵ_m. In Fig. 1, σ_c and ϵ_c are the conductivity and permittivity of the cytoplasm. An inner organelle (e.g., nucleus or mitochondria) with outer radius R_3 and thickness R_3-R_4 is also shown. The corresponding conductivities and permittivities of the organelle membrane and its inner region are denoted by σ_{om}, ϵ_{om}, and σ_{oc}, ϵ_{oc}, respectively. Due to spherical symmetry, the potentials can be expressed as:

$$\phi_{nc}(r,t) = \sum_{i=0}^{\infty} A_i(t) r^i P_i, \tag{1a}$$

$$\phi_{ne}(r,t) = \sum_{i=0}^{\infty} B_{3i}(t) r^i P_i + C_{3i}(t) P_i / r^{i+1}, \tag{1b}$$

$$\phi_c(r,t) = \sum_{i=0}^{\infty} B_{2i}(t) r^i P_i + C_{2i}(t) P_i / r^{i+1}, \tag{1c}$$

$$\phi_m(r,t) = \sum_{i=0}^{\infty} B_{1i}(t) r^i P_i + C_{1i}(t) P_i / r^{i+1}, \tag{1d}$$

$$\phi_o(r,t) = -E_0(t) + \sum_{i=0}^{\infty} D_i(t) P_i / r^{i+1}, \tag{1e}$$

where $\phi_o(r,t)$, $\phi_m(r,t)$, $\phi_c(r,t)$, $\phi_{om}(r,t)$ and $\phi_{oc}(r,t)$ are the potentials at the outer region, the plasma membrane, the cytoplasm, the organelle membrane, and the organelle interior. P_j is the jth order Legendre polynomial, and $E_0(t)$ the externally applied electric field. Also, $A_i(t)$, $B_{1i}(t)$, $B_{2i}(t)$, $B_{3i}(t)$, $C_{1i}(t)$, $C_{2i}(t)$, $C_{3i}(t)$, and $D_i(t)$ are the coefficients of the Legendre series expansions that can be determined by applying matching boundary conditions at the interfaces of the three regions. Here, the Laplace (instead of Poisson's equation) has been used on the assumption that charge inequalities arising from ionic transport during electroporation process can be ignored on the short time scales. As will be shown later, the current flows are not very large and so charge transfer during the ultrashort time scales of interest here ($\sim$5 ns), are indeed minimal. Invoking continuity in the potential and current density then leads to the following boundary conditions:

$$\phi_o(r,t)|_{R_1} = \phi_m(r,t)|_{R_1}, \tag{2a}$$

$$\phi_m(r,t)|_{R_2} = \phi_c(r,t)|_{R_2}, \tag{2b}$$

$$\phi_c(r,t)|_{R_3} = \phi_{om}(r,t)|_{R_3}, \tag{2c}$$

$$\phi_{om}(r,t)|_{R_4} = \phi_{oc}(r,t)|_{R_4}, \tag{2d}$$

$$\sigma_o E_r^o(t) + \epsilon_o \left.\frac{\partial E_r^o(t)}{\partial t}\right|_{R_1} = \sigma_m E_r^m(t) + \epsilon_m \left.\frac{\partial E_r^m(t)}{\partial t}\right|_{R_1}, \tag{2e}$$

$$\sigma_m E_r^m(t) + \epsilon_m \left.\frac{\partial E_r^m(t)}{\partial t}\right|_{R_2} = \sigma_c E_r^c(t) + \epsilon_c \left.\frac{\partial E_r^c(t)}{\partial t}\right|_{R_2}, \tag{2f}$$

$$\sigma_c E_r^c(t) + \epsilon_c \left.\frac{\partial E_r^c(t)}{\partial t}\right|_{R_3} = \sigma_{om} E_r^{om}(t) + \epsilon_{om} \left.\frac{\partial E_r^{om}(t)}{\partial t}\right|_{R_3}, \tag{2g}$$

$$\sigma_{om} E_r^{om}(t) + \epsilon_{om} \left.\frac{\partial E_r^{om}(t)}{\partial t}\right|_{R_4} = \sigma_{oc} E_r^{oc}(t) + \epsilon_{oc} \left.\frac{\partial E_r^{oc}(t)}{\partial t}\right|_{R_4}. \tag{2h}$$

Here $E_r = -\partial\phi/\partial t$ is the radial electric field. Due to electroporation, the parameters $\sigma_m(t)$, $\epsilon_m(t)$, $\sigma_{om}(t)$, and $\epsilon_{oc}(t)$ are all time dependent. For self-consistency, the time dependence of these electrical transport parameters has to be obtained and taken into consideration. This was carried out here by coupling the Smoluchowski equation (SE) for the growth and decay of pores. Details of the SE, its application to electroporation and dynamical conductivity have been addressed in a series of recent papers [30,53,54] by our group, and will not be reviewed here. In essence, the pore area and effective membrane conductivity [$=\sigma_m(t)$] become time dependent. Taking this into account, Eq. (1) and Eq. (2) can finally be cast into the following form:

$$K \begin{pmatrix} A(t+\Delta t) \\ B_1(t+\Delta t) \\ B_2(t+\Delta t) \\ B_3(t+\Delta t) \end{pmatrix} = \begin{pmatrix} f_1(t) \\ f_2(t) \\ f_3(t) \\ f_4(t) \end{pmatrix}, \tag{3}$$

where K is a 4×4 coefficient matrix, while $C_j(t+\Delta t)$ and $D(t+\Delta t)$ are updated at each time step based on the various values $A(t+\Delta t)$ and $B_j(t+\Delta t)$, for $j=1,2,3$. The vector $f(t)$ on the right side of Eq. (3), are known functions that are updated every time step.

Solving Eqs. (2a)–(2h) and (3) yields the transmembrane potential and electric field at a chosen "patch" on the cell membrane. In the present case, the patch was taken to be on the polar axis.

B. Molecular dynamics simulations

The molecular dynamics (MD) scheme was used to probe electric-field-induced effects on a typical membrane. This method is superior to continuum approaches. Some of the advantages are as follows: (i) Inclusion of the collective, many-body interaction potentials at the nanoscale level, (ii) dynamical screening, (iii) avoidance of the "mean-field" approximations, (iv) a natural inclusion of noise and statistical fluctuations, (v) self-consistent and dynamical transport calculations without arbitrary fitting parameters, and (vi) easy incorporation of arbitrary defects and nonuniformities, as well as complex geometries.

In early work, Veneble *et al.* [56] and Egberts *et al.* [57] applied this technique to dipalmitoylphosphatidylcholine (DPPC) bilayers. Various other studies of lipid bilayer systems have since been reported [58–61]. MD simulations rely on the application of classical Newtonian mechanics for the dynamical movement of ions and neutral atoms, taking account of the many-body interactions within a realistic molecular representation of the biosystem [62–65]. Thus, for example, a segment of the lipid bilayer membrane or a channel protein is first constructed taking account of the initial geometric arrangement of all the atoms and their bonding angles. Regions of water containing user-specified ion den-

sities are then defined on either side of the membrane to form the total simulation space. In water-lipid system, simple point charge (SPC) is preferred as the water model because it has a better chemical potential in mixed systems.

Initial velocities, temperature and pressure are set for all particles. In order to prevent the system energies from increasing with time due to the dynamic acceleration, velocities are typically rescaled periodically by coupling the system to a constant temperature bath [66].

In our study, the GROMACS (Groningen Machine for Chemical Simulations) package in NpT ensemble [67–69] was used for the MD simulations of field-induced membrane effects. The dipalmitoyl-phosphatidyl-choline (DPPC) membrane was chosen, and the force fields for membrane molecular motion taken from the literature [65]. The system was coupled using a semi-isotropic Berendsen pressure coupling of 1 atmosphere with compressibility of 4×10^{-5} on x and y direction, and zero on z direction. A heat bath of 323 K is chosen to retain the liquid phase of the membrane [70]. The algorithms for pressure and temperature control were those discussed by Allen and Tildesly [62]. A 4 fs time step was used with algorithm outlined by Berendsen *et al.* [71,72] to constrain all the bond lengths within the lipids and on the water geometry. A group based twin cutoff scheme was employed for the nonbonded interactions, with cutoff radii of 0.9 nm for both the Lennard-Jones and Van der Waals interaction calculations. The particle-mesh Ewald (PME) scheme was applied for long-range electrostatic interactions. Periodic boundaries were applied, and the simulations carried out under constant pressure conditions. This method [66] allows the simulation box size to change so that the internal virial matches the external pressure.

For PS externalization studies, a dipalmitoyl-phosphatidyl-serine (DPPS) lipid molecule was embedded in a membrane with 127 coarse-grained DPPC molecules (arranged on a uniform 8×8 square grid) and 7310 simple point charge (SPC) waters. The DPPS was a megamolecule similar to DPPC as shown in Fig. 2, but with negatively charged serine replacing choline. The megamolecules were treated as single Lennard-Jones centers, with the energy and distance parameters for each subgroup taken from the literature [63,67,68]. Such coarse-grained models have been used recently [41,73–75] to significantly reduce the computational burden associated with an all-atom approach. Here a coarse-grained model has been used for the lipid membrane with the all-atom SPC model for the water molecules. Ideally, an all-atom model is the most accurate, and MD computations using this approach have been pioneered by Marrink, Mark, Knecht, and Tieleman [40,42,43]. However, an all-atom model is computationally prohibitive. Hence, as a more manageable alternative, coarse-grained models have been proposed [41,73–75]. Such coarse-grained models have been found to yield fairly accurate predictions while significantly reducing the computational burden. Here our primary interest is on the cell membrane response to an external electric field leading to pore formation and possible PS externalization. Hence, it is important to include all molecular features that are influenced by the external electric field. Dipoles are important in this regard, and must be included for both the membrane and water molecules. The coarse-grained model

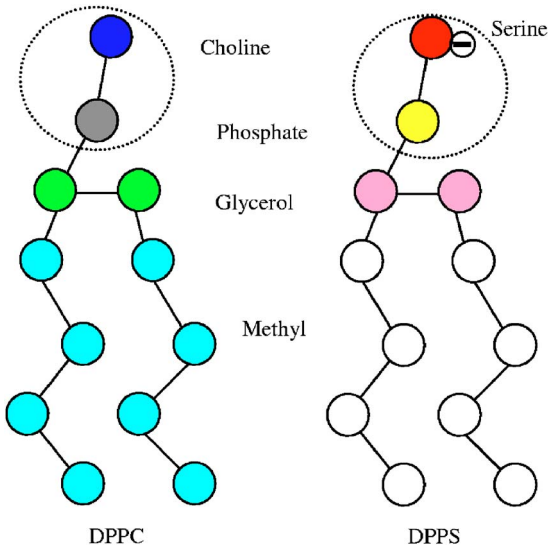

FIG. 2. (Color online) The coarse-grained representation of dipalmitoyl-phosphatidyl-choline (DPPC) and dipalmitoyl-phosphatidyl-serine (DPPS) lipid molecules.

for the lipid layer includes the dipoles and hence is computationally efficient without compromising the inherent physics. However, one cannot simply apply a coarse-grained model for water in the present context. Instead, an all-atom water model becomes necessary for the following reasons. First, only an all-water model naturally builds in the physical effects of polarization, dynamic screening, and field-dependent orientational variations. Also, coarse-grained water models would have a large effective mass and spherical radius, thereby preventing the physical penetration of individual water molecules into membrane nanopores. Since the focus is on pore formation, facilitated by the entry of water molecules into the lipid membrane, an all-atom water model becomes necessary. Finally, as shown in the next section, our chosen hybrid model yields good agreement with available experimental data and is validated against other reports in the literature. For completeness it may be mentioned that mixing the coarse-grained membrane representation with the atomistic water model has some limitations. For example, the entropic contributions are not equivalently treated. However, the primary effect in our case arises from the electrostatic interactions. Hence, we have been careful to incorporate time-dependent electric fields, and all electrostatic interactions arising from distributed dipoles and ions.

III. RESULTS AND DISCUSSION

For concreteness, human Jurkat T lymphocytes were chosen for the simulation studies based on the reported studies of PS externalization for this cell type. This cell line has been used in recent experiments within our group and elsewhere. The relevant parameters used are given in Table I. The listed conductivity is for intact membranes, but becomes time-dependent upon pore formation.

Simulation results of the time dependent transmembrane potential for a cell subjected to a trapezoidal pulse are given

TABLE I. Parameters used for the simulation.

Conductivities(S/m):	
Environment	0.6
Cell membrane	5.3×10^{-6}
Cytoplasm	0.13
Nuclear envelope	4.3×10^{-3}
Nucloplasm	0.18
Dielectric constant:	
Environment	80.0
Cell membrane	7.0
Cytoplasm	60.0
Nuclear envelope	22.8
Nucleoplasm	120.0
Geometry parameters:	
Radius of the simulation region	10 μm
Radius of cell	5.12 μm
Thickness of cell membrane	7 nm
Radius of nucleus	4.4 μm
Thickness of nucleus envelope	40 nm

in Fig. 3. A coupled scheme based on the Laplace and Smoluchowski equations was used for the calculations. The external, averaged electric field pulse was taken to be 0.01 V/nm in magnitude, with rise and fall times of 1.5 ns and 1.5 ns, respectively, and a 10 ns ON-time. Such pulses are routinely used for experimental research in our group [2,29]. During the initial 500 ns of the simulation (as shown in Fig. 3), no external pulse was applied. This was done to allow the system to reach an initial steady state with an equilibrium distribution of nanopores within the membranes in keeping with the Smoluchowski-based continuum model [29,53]. A transient overshoot of the transmembrane potential is predicted in Fig. 3. The overshoot trend agrees very well with a recent experimental report [76]. The time-dependent electric field values across the plasma membrane obtained from these time-dependent results were used as realistic inputs for the MD simulations. Thus, this approach effectively connected our macroscopic, time dependent transmembrane voltage to the MD scheme, allowing for accurate nanoscale study of membrane breakdown by a large external voltage.

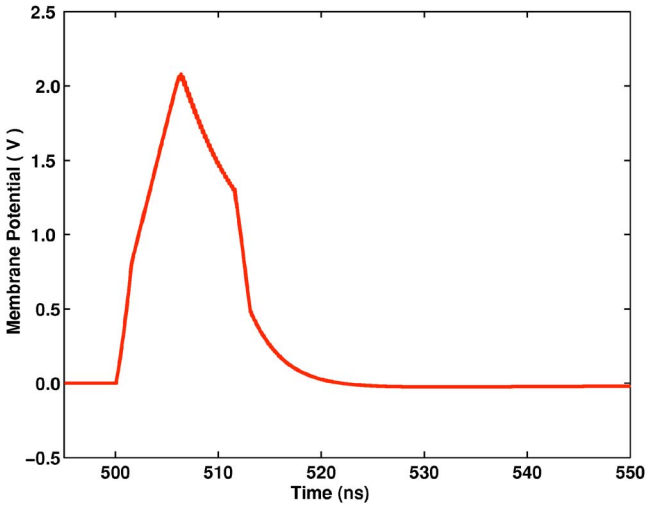

FIG. 3. (Color online) Transmembrane voltage vs time for plasma membrane when applied E field is 0.01 V/nm with a 10 ns duration, a 1.5 ns rise time, and 1.5 ns fall time.

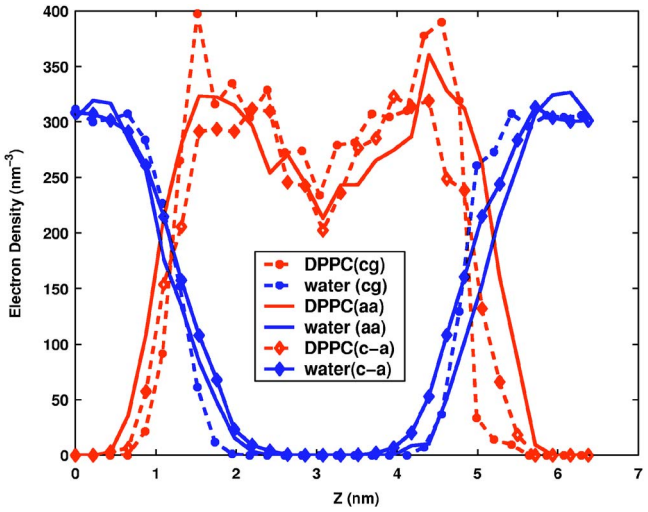

FIG. 4. (Color online) The spatial electron distribution for three different models: the coarse-grain (cg) model, the all atom (aa) model, and the hybrid model (c-a).

As regards the MD study, we adopted the approach proposed by Tieleman *et al.* [43], and started with an equilibrium stable system containing 127 DPPC lipids, 1 DPPS molecule and 7310 water molecules and transforming it into our coarse-grain model. For simplicity and purposes of validation, our MD simulations were first carried out at zero electric field. Part of the objective was to compare the current hybrid model (i.e., coarse-grained representation of the lipid membrane with an all-atom SPC model for the water) with an all-atom approach. Ideally, under these zero field conditions, one does not expect water molecules to penetrate the membrane. This is validated and clearly seen from our MD result for the spatial electron density distribution shown in Fig. 4. Electron density curves within DPPC and the water molecules obtained from the simulations have been shown for three different cases. (a) For an "all coarse-grained" model denoted by the "cg" curves in Fig. 4. In this case, both the lipid membrane and water were coarse grained. (b) A full "all-atom" implementation denoted by the "aa" curves and (c) the hybrid model with coarse-graining for the lipid membrane and an all-atom representation for the water molecules shown by the "c-a" curves in Fig. 4. The absence of electron density over the central portion of the membrane is indicative of the inability of water molecules to pass through the membrane. These results are also very similar to a recent published report [73]. The close agreement helps validate the present model and its implementation. For additional verification of the present model, molecular dynamics based electroporation simulations at a constant electric field of 0.5 V/nm were also carried out. The results (not shown here) revealed pore formation after about 3.55 ns. This is roughly

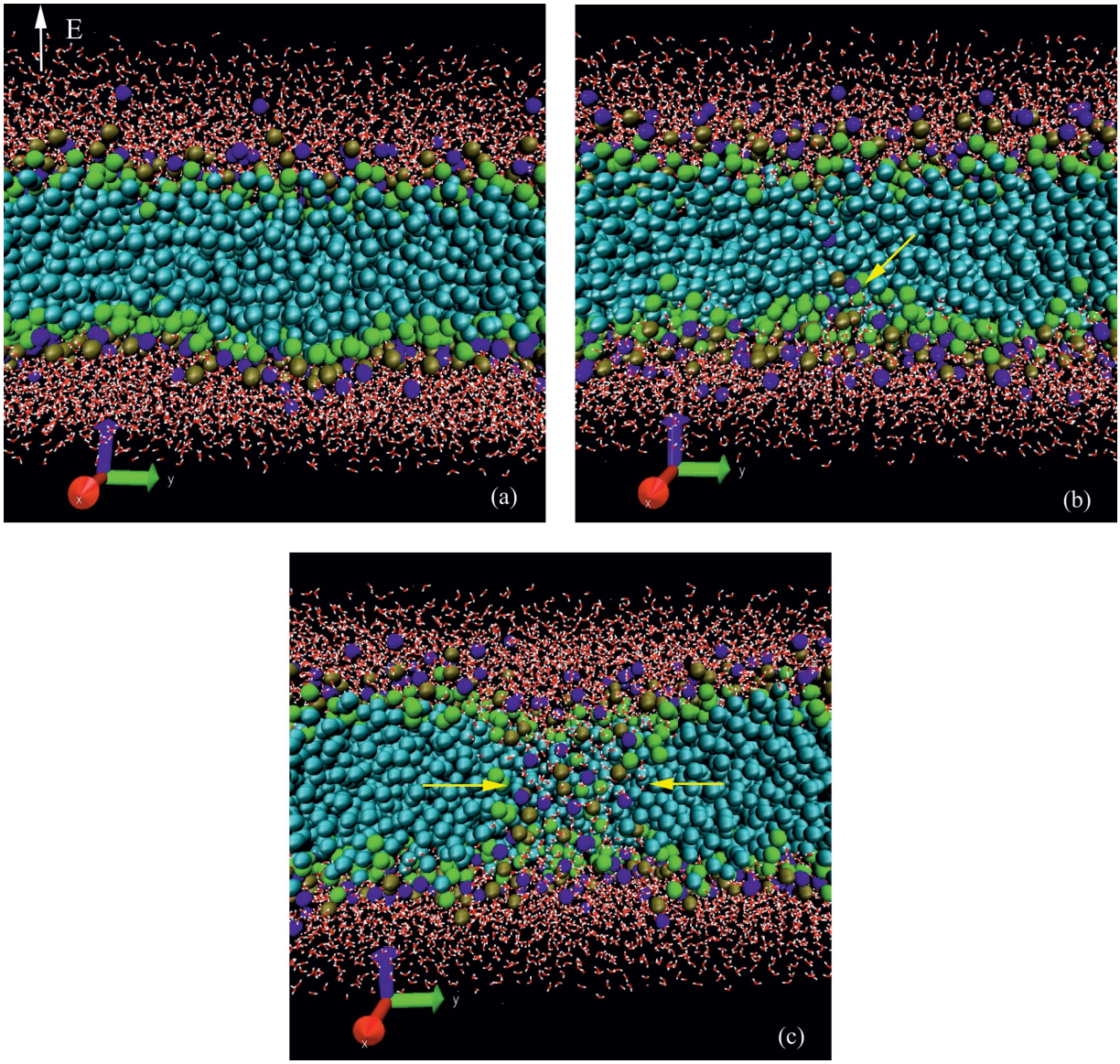

FIG. 5. (Color) MD snapshots of the electroporation process in a DPPC membrane under the E field of Fig. 3. (a) Initial configuration at $t=0$ ns; (b) structural rearrangement begins at the membrane bottom (anode side) at about $t=4.8$ ns; (c) a pore predicted to form at $t=5.3$ ns. The positively polarized choline groups are colored blue, and the negatively polarized phosphatidyl group brown, the glycerol green, the tails cyan. The oxygens in water molecules are red and hydrogens are white.

in keeping with a recent report by Tieleman *et al.* [43] based on a more sophisticated all-atom model for dioleoylphosphatidyl-choline. This lends an additional test of our present method.

Next, the effect of a realistic high-intensity, ultrashort electric field pulse on PS externalization was studied. After performing an energy minimization on our coarse-grained system, the electrical field obtained from Fig. 3 was applied. Snapshots showing the process of membrane configurational change are given in Fig. 5. Figure 5(a) shows the membrane to be well aligned (designated as the $t=0$ ns instant) right after the energy minimization was performed. After about 4.8 ns, some structural rearrangement (i.e., defect formation) begins to form at the anode side (i.e., the membrane bottom) as shown in Fig. 5(b). A pore is then seen to form fairly quickly after the creation of the initial defect. Complete nanopore formation is predicted within about 0.5 ns after the initial structural change. Obviously, most of the time for the electroporation process is taken up by the initial defect formation. A pore, formed at 5.3 ns, is shown in Fig. 5(c).

This result demonstrates a good match between the MD result of Fig. 5, predictions of the continuum model, and actual experimental data [77,78]. A nanopore is predicted to form within about 5–6 ns at these high field intensities. For corroboration and validation under external voltage conditions, a comparison with actual experimental data obtained in our laboratory for a Jurkat cell subjected to a 100 kV/cm nsPEF is presented in Fig. 6. The data is the measured time-dependent shift in luminescent intensity (at a fixed wavelength) from fluorescent dyes embedded in Jurkat cells subjected to the nsPEF. The shift in intensity is directly related to the magnitude of the membrane electric field, since the

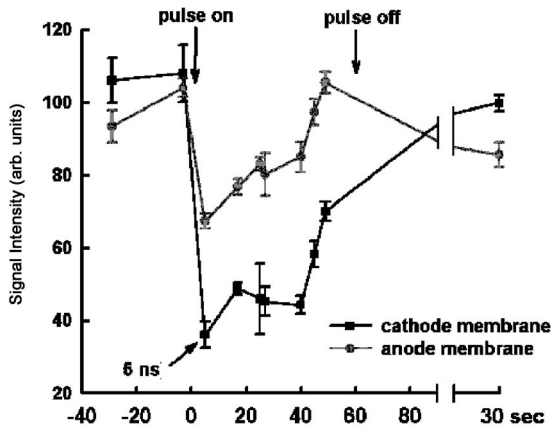

FIG. 6. Experimental data showing the time-dependent fluorescent dye signal in response to a 0.01 V/nm pulse applied to Jurkat cells.

characteristic luminescent spectra of the dye shifts with field based on the linear Stark effect. The two curves shown correspond to measurements taken at the two opposite poles directly facing the anode and cathode, respectively. Slight differences in the two curves arise from the opposing directionality of the initial builtin transmembrane field (i.e., the polarity difference of resting potentials). The initial rapid decrease of fluorescent intensity is a signature of the monotonic transmembrane voltage variation. The slope in Fig. 6 is seen to change after about 6 ns, and the signal begins to recover beyond this time. This is indicative of a poration event and an increased membrane conductance leading to a decrease in transmembrane voltage. The measured time scale for the cellular electroporation event appears to agree well with the simulation result of Fig. 5 and roughly justifies our model.

This result of Fig. 5 also demonstrates that the initial structural rearrangement and dipole re-orientation is a critical step in the electroporation process. Once such an initial breakthrough is achieved, the poration process proceeds relatively quickly. Finally, the poration process has polarity dependence, and begins on the anodic side of a membrane. The related physics can easily be understood by considering the configuration within the DPPC membrane. Figure 7 shows a simple schematic of the membrane lipids with their dipoles

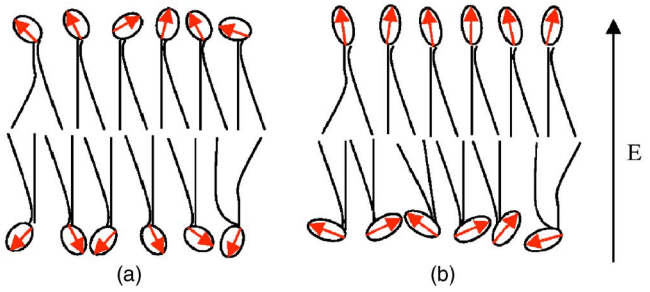

FIG. 7. (Color online) Schematic of the pore initiation process at the DPPC membrane. The arrows present dipoles on the head groups of lipid molecules. (a) Initial configuration without an externally applied field, and (b) the configuration and expected movement of the dipole head groups upon the application of an external electric field.

located at the head groups. For each DPPC chain, the head group contains a dipole with positive charge on choline and negative charge centered on the phosphate group. Initially, with no electric field present, the dipoles are in random thermal motion with the positive charges residing on the outermost portions of the lipid. Thus Fig. 7(a) shows randomly distributed dipoles at the head groups on either side of the membrane as the initial configuration. Electrical field induced defects are initiated by the movement of dipoles on the surface of the membrane. Defects start to form on the anode side of the membrane because positively charged molecules (e.g., choline) on this side are forced to swing around (i.e., reorient in the presence of a strong external electric field) and enter the membrane. This same electrical field, however, when acting on the dipoles located at the cathodic surface merely works to stretch the dipoles without any molecular movement into the membrane volume. Figure 7(b) shows the alignment of dipolar head groups on the anodic side gradually deviating from the equilibrium orientation, and a defect starting to form.

Thus pore formation is predicted to initiate at the membrane pole facing the anode. If PS externalization is pore-driven event, then this process should also start at the anode side. Experimental observations do indicate just such an anode side preference. The electrostatics provides an additional rationale for an anode-side event. Since the PS molecules residing on the inner leaflet are negatively charged, the externally applied electric field will tend to push out PS at the anode side, while pulling it inwards on the cathodic side. Coupling this with an anode-side pore formation event, leads to the collective effect of preferential PS externalization at the anode end. Figure 8 is a simple schematic demonstrating

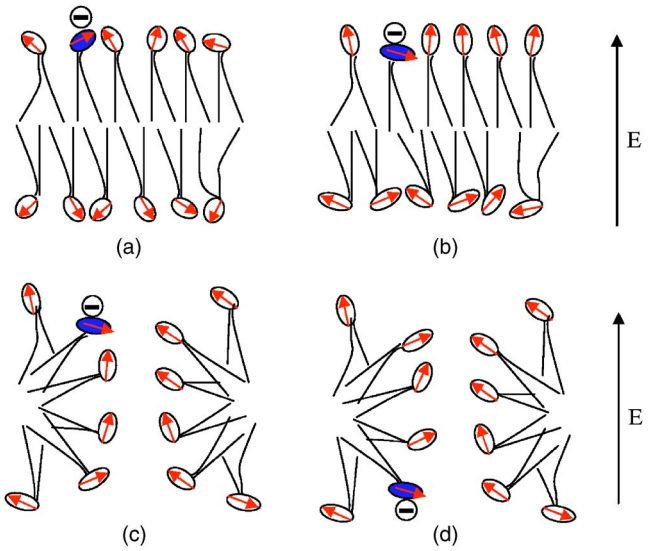

FIG. 8. (Color online) Schematic of the pore initiation process within a DPPC-DPPS membrane. The arrows represent dipoles on the lipid head groups, and the shaded circle denotes the negative DPPS head group. (a) Initial configuration without an externally applied field; (b) expected configuration of the dipole head groups with an external field; (c) nanopore formation with a DPPS molecule close to the pore; and (d) DPPS molecular movement to the outer leaflet of the membrane.

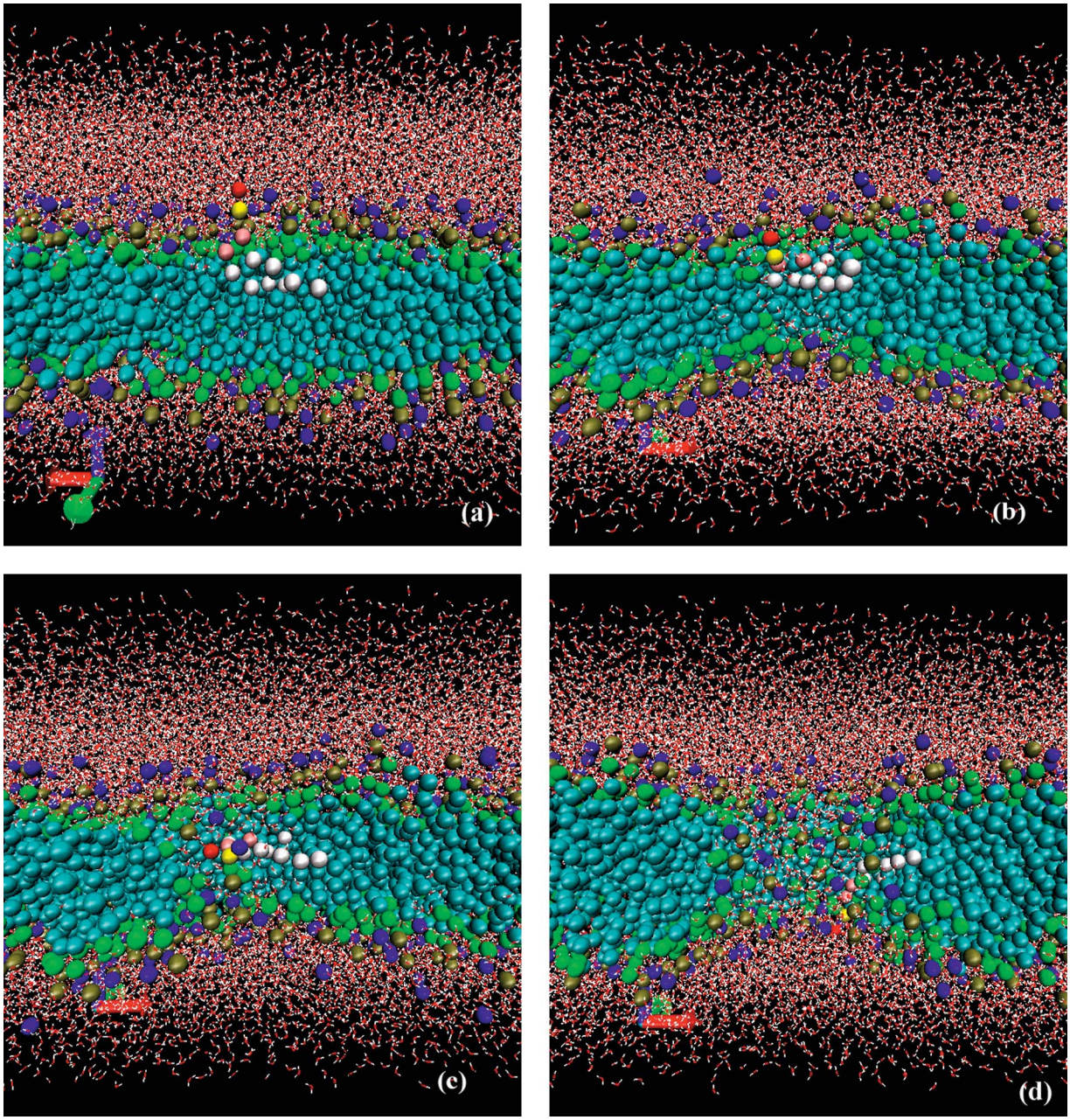

FIG. 9. (Color) Snapshots of the DPPS externalization process at a DPPC membrane. (a) Initial configuration at ~0 ns; (b) a pore forms and DPPS starts to go along the pore wall at ~3.2 ns; (c) DPPS halfway to externalization at ~3.34 ns; and (d) DPPS on the other leaflet of the membrane at ~3.61 ns. The coloring of DPPC is the same as Fig. 5. And for DPPS, the positively polarized choline groups are colored red, and the negatively polarized phosphatidyl group yellow, the glycerol pink, the tails white. The oxygens in water molecules are red and hydrogens are white.

the dynamics. Initially [Fig. 8(a)], the dipoles at the DPPC lipids (shown as arrows) are randomly located, with a negative PS on the inner leaflet. With application of the electric field, the dipoles on the outer layer (anode-side) reorient leading to defect initiation at the outer membrane surface. Eventually a pore forms [Fig. 8(c)], and the negatively charged PS begins to drift and diffuse towards the exterior surface.

Results of MD simulations, shown in Figs. 8(a)–8(d) demonstrate the above more clearly. An initial snapshot of the membrane system is shown in Fig. 9(a), with the PS molecule located on one side of the membrane, opposite the anode. Figure 9(b) shows a pore starting to form with some translocation of the PS chain at 3.2 ns. Due to a large electrostatic force on the PS head group (in the range of ~10–10 N), the chain is dragged halfway to the anode side of the membrane along the wall of the nanopore at about ~3.34 ns as shown in Fig. 9(c). Finally, in Fig. 9(d), the DPPS chain is on the other leaflet of the membrane at ~3.61 ns. The MD simulation thus validates the pore-facilitated, field-assisted mechanism of PS externalization. An important difference between the DPPC-DPPS simula-

tions of Fig. 9 and results for a pure DPPC membrane (Fig. 5) is the shorter time duration for pore formation. Inclusion of a membrane defect in the form of a substitutional DPPS molecule, and the additional membrane force associated with the negative PS charge collectively contribute to the quicker poration.

IV. SUMMARY AND CONCLUSIONS

A combined MD simulator and the time dependent Laplace solver were used to predict the self-consistent cell-membrane response to an ultrashort and high intensity external electric field. The primary goal was to probe the electrically driven PS externalization process. An additional objective was to develop the computational capability of treating the dynamical aspects at the molecular level, without resorting to an all-atom model. The realistic inclusion of a time-dependent electric field in to MD simulations was also achieved. The DPPC and DPPS lipid molecules were represented. Essential features such as the hydrophilic and hydrophobic nature of the lipid chain interactions were included, as were the clustering of water molecules around ions due to the electric field gradients at the microscopic level.

Time dependent details of nanopore formation at membranes in response to a variable electric field were probed. Details of the variable membrane field were computed from a distributed current model applied to the entire cell. Our results showed that nanosized pores could typically be formed within 5–6 ns for spatially averaged external fields of about 0.01 V/nm. The predictions were in very good agreement with recent experimental data. It was shown that defect formation on membranes would begin on the anode side. Finally, it was shown that PS translocation would be a nanopore facilitated event, rather than the result of molecular movement across the transmembrane energy barrier. For high electric fields, the pore could form before the pulse extinction. Under these conditions, both drift and diffusion of the PS molecules from the anode-side, inner leaflet are predicted to occur. At lower intensities or shorter pulse durations, the electric field could still help trigger PS externalization. In such cases, the immediate consequence would be a structural change at the anodic pole. Subsequent molecular diffusive motion aided by the hydrophobic interaction between incoming water and the lipid tails, could then result in a gradual PS leakout to the membrane exterior at longer times.

ACKNOWLEDGMENTS

This work was sponsored in part by the Air Force Office of Scientific Research (No. F49620-01-1-0506) on Bio-Inspired Concepts and an AFOSR-MURI grant (No. F49620-02-1-0320) on Subcellular Responses to Narrowband and Wideband Radio Frequency Radiation. The authors would also like to acknowledge useful and stimulating discussions with J. Weaver (MIT), D. P. Tieleman (Univ. Calgary), E. Neumann (University of Bielefeld), and P. T. Vernier (Univ. S. California).

[1] K. H. Schoenbach, F. E. Peterkin, R. W. Alden, and S. J. Beebe, IEEE Trans. Plasma Sci. **25**, 284 (1997).
[2] K. H. Schoenbach, S. J. Beebe, and E. S. Buescher, Bioelectromagnetics (N.Y.) **22**, 440 (2001).
[3] R. P. Joshi, Q. Hu, R. Aly, K. H. Schoenbach, and H. P. Hjalmarson, Phys. Rev. E **64**, 011913 (2001).
[4] H. Huelsheger, J. Potel, and E. G. Niemann, Radiat. Environ. Biophys. **20**, 53 (1981).
[5] J. C. Weaver, IEEE Trans. Plasma Sci. **28**, 24 (2000).
[6] U. Zimmermann and G. A. Neil, *Electromanipulation of Cell* (CRC, Boca Raton, FL, 1996).
[7] U. Zimmermann, J. Vienken, and G. Pilwat, Bioelectrochem. Bioenerg. **7**, 553 (1980).
[8] M. M. Lo, T. Y. Tsong, M. K. Conrad, S. M. Strittmatter, L. D. Hester, and S. H. Snyder, Nature (London) **310**, 792 (1984).
[9] L. H. Li, M. L. Hensen, Y. L. Zhao, and S. W. Hui, Biophysics (Engl. Transl.) **71**, 479 (1996).
[10] A. K. Banga and M. R. Prausnitz, Trends Biotechnol. **16**, 408 (1998).
[11] E. Eksioglu-Demiralp, S. Kitada, D. Carson, J. Garland, A. Andreef, and J. C. Reed, J. Immunol. Methods **275**, 41 (2003).
[12] M. F. Kalady, M. W. Onaitis, K. M. Padilla, S. Emani, D. S. Tyler, and S. K. Pruitt, Surg. Forum **52**, 225 (2001).
[13] G. Mellitzer, M. Hallonet, L. Chen, and S. L. Ang, Mech. Dev. **118**, 57 (2002).
[14] R. L. Harrison, B. J. Byrne, and L. Tung, FEBS Lett. **435**, 1 (1998).
[15] R. Langer, Nature (London) **392**, s5 (1998).
[16] L. Zhang, L. Li, G. Hoffmann, and R. Hoffman, Biochem. Biophys. Res. Commun. **220**, 633 (1996).
[17] H. Mekid and L. M. Mir, Biochim. Biophys. Acta **1524**, 118 (2001).
[18] C. Ramos and J. Teissie, Biochimie **82**, 511 (2000).
[19] K. H. Schoenbach, R. P. Joshi, R. H. Stark, F. C. Dobbs, and S. J. Beebe, IEEE Trans. Dielectr. Electr. Insul. **7**, 637 (2000).
[20] A. J. H. Sale and W. A. Hamilton, Biochim. Biophys. Acta **148**, 781 (1967).
[21] A. J. H. Sale and W. A. Hamilton, Biochim. Biophys. Acta **163**, 37 (1967).
[22] U. Broggemann, E. C. Roux, J. Hanning, and C. Nicolau, Transfusion (Bethesda, Md.) **35**, 478 (1995).
[23] M. Zeira, P. F. Tosi, Y. Mouneimne, J. Lazarte, L. Sneed, D. J. Volsky, and C. Nicolau, Proc. Natl. Acad. Sci. U.S.A. **88**, 4409 (1991).
[24] L. M. Mir, S. Orlowski, J. B. Jr, and C. Paoletti, Eur. J. Cancer **27**, 68 (1991).
[25] F. Lohr, D. Y. Lo, D. A. Zaharoff, K. Hu, X. Zhang, Y. Li, Y. Zhao, M. W. Dewhirst, F. Yuan, and C. Y. Li, Cancer Res. **61**, 3281 (1984).
[26] M. Ott, J. D. Robertson, V. Gogvadze, B. Zhivotovsky, and S. Orrenius, Proc. Natl. Acad. Sci. U.S.A. **99**, 1259 (2002).
[27] L. Piccotti, M. Buratta, S. Giannini, P. Gresele, R. Roberti, and

L. Corazzi, J. Membr. Biol. **198**, 43 (2004).
[28] S. J. Beebe, P. M. Fox, L. J. Rec, K. Somers, R. H. Stark, and K. H. Schoenbach, IEEE Trans. Plasma Sci. **30**, 286 (2002).
[29] S. J. Beebe, P. M. Fox, L. J. Rec, L. K. Willis, and K. H. Schoenbach, FASEB J. **17**, 1493 (2003).
[30] R. P. Joshi, Q. Hu, K. H. Schoenbach, and S. J. Beebe, Phys. Rev. E **69**, 051901 (2004).
[31] P. T. Vernier, Y. Sun, L. Marcu, C. M. Craft, and M. A. Gundersen, Biophys. J. **86**, 4040 (2004).
[32] P. T. Vernier, Y. Sun, L. Marcu, C. M. Craft, and M. A. Gundersen, FEBS Lett. **572**, 103 (2004).
[33] J. Deng, K. H. Schoenbach, E. S. Buescher, P. S. Hair, P. M. Fox, and S. J. Beebe, Biophys. J. **84**, 2709 (2003).
[34] P. T. Vernier, Y. Sun, L. Marcu, S. Salemi, C. M. Craft, and M. A. Gundersen, Biochem. Biophys. Res. Commun. **310**, 286 (2003).
[35] S. J. Beebe, P. F. Blackmore, J. White, R. P. Joshi, and K. H. Schoenbach, Physiol. Meas **25**, 1077 (2004).
[36] V. F. Pastushenko, Y. A. Chhizmadzhev, and V. B. Arakelyan, Bioelectrochem. Bioenerg. **6**, 53 (1979).
[37] A. Barnett and J. C. Weaver, Bioelectrochem. Bioenerg. **25**, 163 (1991).
[38] V. A. Parsegian, Nature (London) **221**, 844 (1969).
[39] J. Marti and F. S. Csajka, Europhys. Lett. **61**, 409 (2003).
[40] S. J. Marrink, E. Lindahl, O. Edholm, and A. E. Mark, J. Am. Chem. Soc. **123**, 8638 (2004).
[41] S. J. Marrink, A. H. de Vries, and A. E. Mark, J. Phys. Chem. **108**, 750 (2004).
[42] V. Knecht, M. Muller, M. Bonn, S. J. Marrink, and A. Mark, J. Chem. Phys. **122**, 024704 (2005).
[43] D. P. Tieleman, H. Leontiadou, A. E. Mark, and S. J. Marrink, Comput. Phys. Commun. **125**, 6382 (2003).
[44] Q. Hu, S. Viswanadham, R. P. Joshi, K. H. Schoenbach, S. J. Beebe, and P. F. Blackmore, Phys. Rev. E **71**, 031914 (2005).
[45] B. Verhoven, R. A. Schlegel, and P. Williamson, J. Exp. Med. **182**, 1597 (1995).
[46] M. Seigneuret and P. F. Devaux, Proc. Natl. Acad. Sci. U.S.A. **81**, 3751 (1984).
[47] F. Basse, J. G. Stout, P. J. Sims, and T. Wiedmer, J. Biol. Chem. **271**, 17205 (1996).
[48] P. Comfurius, P. Williamson, E. F. Smeets, R. A. Schlegel, E. M. Bevers, and R. F. Zwaal, Biochemistry **35**, 7631 (1996).
[49] K. Balasubramaniun and A. J. Schroit, Annu. Rev. Physiol. **65**, 701 (2003).
[50] I. R. Miller, Bioelectrochemistry **57**, 138 (2002).
[51] D. Popescu and G. Victor, Bioelectrochem. Bioenerg. **25**, 105 (1983).
[52] J. Jiang, B. F. Serinkan, Y. Y. Tyurina, G. G. Borisenko, Z. Mi, P. D. Robbins, A. J. Schroit, and V. E. Kagan, Free Radic Biol. Med. **35**, 814 (2003).
[53] R. P. Joshi, Q. Hu, K. H. Schoenbach, and H. P. Hjalmarson, Phys. Rev. E **65**, 041920 (2002).
[54] R. P. Joshi, Q. Hu, and K. H. Schoenbach, IEEE Trans. Plasma Sci. **32**, 1677 (2004).
[55] C. Grosse and H. P. Schwan, Biophys. J. **63**, 1632 (1992).
[56] R. M. Venable, Y. Zhang, B. J. Hardy, and R. W. Pastor, Science **262**, 223 (1993).
[57] E. Egberts, S. Marrink, and H. J. C. Berendsen, Eur. Biophys. J. **22**, 423 (1993).
[58] H. E. Alper, D. Bassolino, and T. R. Stouch, J. Chem. Phys. **98**, 9798 (1993).
[59] H. Heller, M. Schaefer, and K. Schulten, J. Phys. Chem. **97**, 8343 (1993).
[60] J. J. L. Cascales, J. G. de la Torre, S. J. Marrink, and H. J. C. Berendsen, J. Chem. Phys. **104**, 2713 (1996).
[61] D. P. Tieleman and H. J. C. Berendsen, J. Chem. Phys. **105**, 4871 (1996).
[62] M. P. Allen and D. J. Tildesley, *Computer Simulations of Liquids* (Clarendon Press, Oxford, 1987).
[63] E. Egberts and H. J. C. Berendsen, J. Chem. Phys. **89**, 3718 (1988).
[64] W. F. van Gunsteren and H. J. C. Berendsen, Angew. Chem., Int. Ed. Engl. **29**, 992 (1990).
[65] H. J. C. Berendsen, J. P. M. Postma, W. F. Gunsteren, and J. Hermans, *Intermolecular Forces*, edited by B. Pullman (Reidel, Dordrecht, 1981).
[66] H. J. C. Berendsen, J. P. M. Straatsma, W. F. van Gunsteren, A. DiNola, and J. R. Haak, J. Phys. Chem. **81**, 3684 (1984).
[67] D. van der Spoel, A. R. van Buuren, E. Apol, P. J. Meulenhoff, D. P. Tieleman, A. L. Sijbers, R. van Drunen, and H. J. C. Berendsen, Gromacs User Manual Version 1.2, 1996.
[68] H. J. C. Berendsen, D. van der Spoel, and R. van Drumen, Comput. Phys. Commun. **91**, 43 (1995).
[69] E. Lindahl, B. Hess, and D. van der Spoel, J. Mol. Model. **7**, 306 (2001).
[70] D. Tieleman, S. J. Marrink, and H. J. C. Berendsen, Biochim. Biophys. Acta **1331**, 235 (1997).
[71] W. F. van Gunsteren and H. J. C. Berendsen, Mol. Phys. **34**, 1131 (1977).
[72] J. P. Ryckaert, G. Ciccotti, and H. J. C. Berendsen, J. Comput. Phys. **25**, 327 (1977).
[73] C. F. Lopez, P. B. Moore, J. C. Shelley, M. Y. Shelley, and M. L. Klein, Comput. Phys. Commun. **147**, 1 (2002).
[74] M. Muller, K. Katsov, and M. Schick, J. Polym. Sci., Part B: Polym. Phys. **41**, 1441 (2003).
[75] B. Smit, P. A. Hilbers, K. Esselink, L. A. M. Rupert, N. M. V. Os, and A. G. Schlijper, Nature (London) **348**, 624 (1990).
[76] W. Meier, A. Graff, A. Diederich, and M. Winterhalter, Phys. Chem. Chem. Phys. **2**, 4559 (2000).
[77] J. Kolb (private communication).
[78] W. Frey, J. A. White, R. O. Price, P. F. Blackmore, R. P. Joshi, S. J. Beebe, R. Nuccitelli, K. H. Schoenbach, and J. F. Kolb (unpublished).